Nuclear Engineering and Design 240 (2010) 2877–2883

Contents lists available at ScienceDirect

Nuclear Engineering and Design

journal homepage: www.elsevier.com/locate/nucengdes

A coupling methodology for mesoscale-informed nuclear fuel performance codes

Michael Tonks[a,*], Derek Gaston[a], Cody Permann[b], Paul Millett[a], Glen Hansen[a], Dieter Wolf[b]

[a] Fuel Modeling and Simulation, Idaho National Laboratory, P.O. Box 1625, Idaho Falls, ID 83415-3840, United States
[b] Center for Advanced Modeling and Simulation, Idaho National Laboratory, P.O. Box 1625, Idaho Falls, ID 83415-3840, United States

ARTICLE INFO

Article history:
Received 23 February 2010
Received in revised form 1 June 2010
Accepted 4 June 2010

MSC:
65N30
68N99
65H10
74S05
74A30

ABSTRACT

This study proposes an approach for capturing the effect of microstructural evolution on reactor fuel performance by coupling a mesoscale irradiated microstructure model with a finite element fuel performance code. To achieve this, the macroscale system is solved in a parallel, fully coupled, fully-implicit manner using the preconditioned Jacobian-free Newton Krylov (JFNK) method. Within the JFNK solution algorithm, microstructure-influenced material parameters are calculated by the mesoscale model and passed back to the macroscale calculation. Due to the stochastic nature of the mesoscale model, a dynamic fitting technique is implemented to smooth roughness in the calculated material parameters. The proposed methodology is demonstrated on a simple model of a reactor fuel pellet. In the model, INL's BISON fuel performance code calculates the steady-state temperature profile in a fuel pellet and the microstructure-influenced thermal conductivity is determined with a phase field model of irradiated microstructures. This simple multiscale model demonstrates good nonlinear convergence and near ideal parallel scalability. By capturing the formation of large mesoscale voids in the pellet interior, the multiscale model predicted the irradiation-induced reduction in the thermal conductivity commonly observed in reactors.

Published by Elsevier B.V.

1. Introduction

As light water reactor fuel undergoes irradiation, the neutron flux and temperature gradient cause fission products and porosity to form and migrate within the pellet (Olander, 1976). This local restructuring of the fuel microstructure results in significantly different local material properties, including thermal conductivity, elastic constants and density (Allison et al., 1993). Ultimately, these properties impact power generation and fuel pellet/cladding interaction, which is a consideration in fuel failure.

Fuel performance codes attempt to consider the effect of microstructure evolution on the macroscale fuel behavior to assist in the design of reactors. These models, such as those seen in Allison et al. (1993), are typically based on empirical fits of experimental data and do not explicitly model the microstructural changes. Therefore, while they can accurately interpolate within understood conditions they cannot accurately extrapolate to new conditions. A phenomenological model of reactor fuel must directly consider microstructural changes to accurately describe the macroscale behavior.

Various models have been developed that predict radiation-induced microstructural evolution. These models represent the microstructure at the mesoscale, resolving grains, voids and bubbles but not individual atoms nor point defects. Tikare and Holm (1998) and Oh et al. (2009) use the Monte Carlo Potts model to describe the evolution of microstructure with existing voids and bubbles. Rokkam et al. (2009) develop a phase field model to predict the nucleation and growth of voids during irradiation. Mesoscale models also provide a mechanism for predicting the effect of irradiation on material properties such as thermal conductivity (Millett et al., 2008). However, the computational expense of employing a mesoscale approach to model a macroscale fuel pellet is prohibitively large, due to the large number of degrees of freedom involved.

The effect of radiation-induced microstructural evolution can be considered at the macroscale by coupling mesoscale calculations to a finite element (FE) fuel performance code. Because FE discretizations only consider the material behavior at integration points, a coupled multiscale model need only resolve the microstructure at these specific points, thus reducing the computational cost of the simulation significantly. Linking between spatial scales is relatively common (Bochev et al., 2004; Yu and Fish, 2002; Michopoulos et al., 2005). However, linking mutually dependent (or coupled) multiscale simulations is more challenging, since operator splitting may result in both stability and accuracy issues (Ropp et al., 2004; Ropp and Shadid, 2005).

* Corresponding author.
E-mail addresses: Michael.Tonks@inl.gov (M. Tonks), Derek.Gaston@inl.gov (D. Gaston), Cody.Permann@inl.gov (C. Permann), Paul.Millett@inl.gov (P. Millett), Glen.Hansen@inl.gov (G. Hansen), Dieter.Wolf@inl.gov (D. Wolf).

0029-5493/$ – see front matter. Published by Elsevier B.V.
doi:10.1016/j.nucengdes.2010.06.005

In the approach proposed here, the Jacobian-free Newton Krylov (JFNK) method (Knoll and Keyes, 2004) is utilized to solve the coupled nonlinear problem. The mesoscale model is solved within the JFNK function evaluation to provide closure for the FE fuel performance code. The FE model provides the current state conditions for the solution of the mesoscale model, which then returns a required value (Beaudoin et al., 1993; Habraken and Duchene, 2004). Coupling the scales within the JFNK function evaluation solves both problems simultaneously and in a self-consistent fashion. It also provides strong convergence of the composite solution, at the cost of expensive function evaluations. The concept of using JFNK in this manner to bridge scales was first proposed by Knoll et al. (2009) to accelerate reactor neutronics calculations.

This paper proposes a general methodology to couple a mesoscale irradiated microstructure model with a FE fuel performance code, stressing the numerical aspects of the scale-bridging approach. The approach is demonstrated on a simplified model of heat conduction in an irradiated fuel pellet. In this model, the Idaho National Laboratory's BISON fuel performance code[1] is used to determine the temperature throughout the pellet using a parallel preconditioned JFNK algorithm, while a phase field mesoscale model (Rokkam et al., 2009) calculates the thermal conductivity in an irradiated microstructure at each integration point. To the authors' knowledge, this paper details the first application of parallel preconditioned JFNK as a means of bridging macro- and mesoscale calculations for reactor fuel performance.

This work begins in Section 2 by summarizing the multiscale model methodology, discussing the approach and the numerical requirements. Section 3 demonstrates the approach on a simplified model of a fuel pellet. First, the simple model is presented where the macroscale problem description, the mesoscale model, and the coupling approach is summarized. Initial results from the multiscale model are then presented. Section 4 concludes the paper and suggests future work.

2. Multiscale model methodology

To represent the effect of the evolving microstructure on the behavior of an irradiated fuel pellet without resolving the entire pellet at the mesoscale, a FE fuel performance code is fully coupled with a mesoscale irradiated microstructure model. The fuel pellet is described by the FE model, including the geometry and boundary and initial conditions, while the mesoscale model resolves the microstructure at the integration points on the FE mesh.

To define the multiscale problem, the domain is divided into coarse and fine spaces. The coarse space is the engineering-scale domain that spans the complete problem geometry, while the fine space, i.e., the mesoscale model, exists only at the integration points. Further, the spatial projection of fine space is assumed to be of measure zero in the coarse space. Given current operating conditions from the macroscale, such as temperature, radiation dose and dose rate at a specific time t, the mesoscale model evolves the microstructure to arrive at the current time. Rather than calculate average values such as stress or temperature directly at the mesoscale, the mesoscale model provides effective macroscale material parameters determined by testing the current microstructure, e.g., the average temperature is not calculated at the mesoscale, but rather the effective thermal conductivity. The system of equations defining the problem can be summarized with the residual equation

$$\mathbf{F}(\mathbf{x}, \mathbf{p}^e) = \mathbf{0}, \tag{1}$$

where $\mathbf{F}$ is the residual vector, $\mathbf{x}$ is the solution vector and $\mathbf{p}^e$ is a vector containing all the effective material properties determined by the mesoscale model.

The microstructure, and therefore the material parameters, vary spatially at the mesoscale. However, this mesoscale spatial variation is negligible at the macroscale, giving a single effective material parameter in the coarse space. The appropriate method with which to calculate an effective material property over a mesoscale microstructure depends on the property. For example, the effective density is equal to the mean mesoscale density, while the effective thermal conductivity is calculated by testing the ability of the microstructure to conduct heat in specific directions (Millett et al., 2008).

The nonlinear system defined by (1) is solved via Newton iteration. Traditional Newton methods require the Jacobian of the residual equation, which is not available when the material parameters are determined from a mesoscale model. Therefore, the JFNK algorithm, which does not require the Jacobian, is employed to solve the system.

Newton methods (including JFNK) are based on a truncated Taylor series

$$\mathbf{F}(\mathbf{x} + \Delta\mathbf{x}, \mathbf{p}^e) \approx \mathbf{F}(\mathbf{x}, \mathbf{p}^e) + \Delta\mathbf{x}\frac{\partial \mathbf{F}(\mathbf{x}, \mathbf{p}^e)}{\partial \mathbf{x}}, \tag{2}$$

in which the higher order derivative terms are neglected. The accuracy of this approximation, and therefore the convergence of the nonlinear solution, improves for small higher order derivatives. Random noise in the function is of particular concern, since it results in large higher order derivatives. Both the Potts (Tikare and Holm, 1998; Oh et al., 2009) and the phase field irradiated microstructure (Rokkam et al., 2009) models can be stochastic, leading to random noise in the calculated effective material properties $\mathbf{p}^e$. The noise is reduced by increasing the mesoscale domain size, but this strategy is generally computationally infeasible, as demonstrated in Section 3.3.

As an alternative means of reducing the random noise, a multidimensional dynamic curve-fitting process is used between the length scales. Here, using a least mean squares algorithm, all values of $\mathbf{p}^e$ calculated by the mesoscale model are fit with a polynomial surface. The macroscale model uses values obtained from the fit, $\mathbf{p}^e_{\text{fit}}$, where each value calculated by the mesoscale model is used to refine the fit. The fit is recalculated at the start of each nonlinear iteration, and gradually improves in accuracy as more values are calculated by the mesoscale model. Further, the dynamic fit records locations of previously performed mesoscale calculations, allowing one to economize solution time by reusing previous values if they are "sufficiently close" to prior calculations. Most importantly, the polynomial fit provides the required smoothness while still being based on values calculated by the mesoscale model.

To summarize the algorithm, a fuel pellet is represented with a macroscale FE model. At each time step, the JFNK algorithm is used to solve the nonlinear system. During the nonlinear convergence process, the mesoscale model evolves the microstructure at the current conditions at each integration point and determines effective material parameter values $\mathbf{p}^e$. These parameters are fit with a polynomial surface, which provides the parameter values $\mathbf{p}^e_{\text{fit}}$ to the FE model. This process is repeated, providing more calculated values to improve the fit, until the solution converges. The evolved mesoscale microstructure at each integration point becomes the initial microstructure at the next time step. See Fig. 1 for a schematic of the proposed multiscale methodology.

3. Simplified multiscale fuel pellet model

To demonstrate the multiscale approach summarized in the previous section, a simplified multiscale model of an irradiated fuel

[1] BISON is built upon INL's MOOSE: a parallel, nonlinear, computational framework (Gaston et al., 2009).

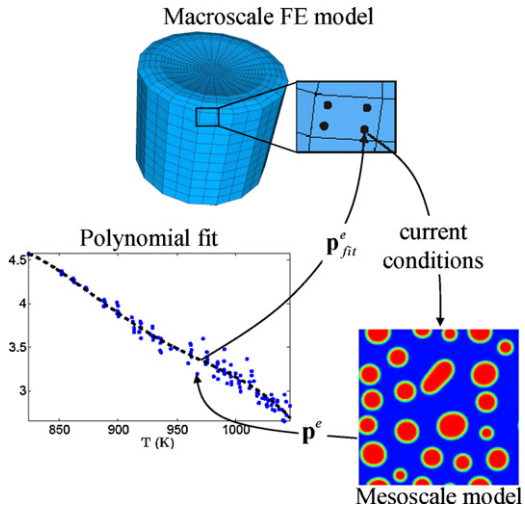

Fig. 1. Schematic of the the proposed multiscale methodology. At the current conditions, the mesoscale model determines effective parameter values $\mathbf{p}^e$ which are fit with a polynomial surface at each nonlinear iteration. The macroscale FE model obtains values of $\mathbf{p}^e_{\text{fit}}$ from the latest fit.

pellet is presented. The dished pellet has a diameter of 8.26 mm and a height of 6.75 mm. In the simple model, the steady-state temperature profile is determined in the fuel pellet using INL's BISON FE code for a single nonlinear solution. At each integration point, the mesoscale phase field model (Rokkam et al., 2009) evolves the microstructure at the current integration point temperature and calculates the effective thermal conductivity. This value is then used by the FE model to determine the temperature for the next nonlinear iteration. Both the macroscale fuel pellet representation and the mesoscale model of the fuel material are significant simplifications of actual fuel pellet behavior, as the purpose of this preliminary work is to develop and demonstrate the multiscale methodology and not to develop an accurate fuel model.

The engineering and mesoscale models are summarized in Sections 3.1 and 3.2, respectively, and the coupling between the models is discussed in Section 3.3. Section 3.4 investigates the numerical performance of the model and Section 3.5 presents initial results.

3.1. Fuel pellet model

Heat conduction within the simplified fuel pellet is defined by

$$\begin{array}{ll} \nabla\cdot\mathbf{q}-Q=0 & T\in\Omega,\\ T=T_C & T\in\Gamma^C,\\ \mathbf{n}\cdot\mathbf{q}=0 & T\in\Gamma^T\cup\Gamma^B,\\ T(t=0)=T_0 & T\in\Omega, \end{array} \tag{3}$$

where T is the internal temperature, the density is assumed constant and fission reactions are assumed to generate heat at a uniformly distributed constant rate, Q. In this expression, Ω denotes the fuel pellet, Γ^T denotes the top and Γ^B denotes the bottom boundary of the fuel pellet, and Γ^C denotes the outer circumferential fuel pellet boundary such that $\Gamma=\Gamma^T\cup\Gamma^B\cup\Gamma^C$. The heat flux $\mathbf{q}$ within the pellet Ω may be written as

$$\mathbf{q}=-k\nabla T, \tag{4}$$

where k is the isotropic thermal conductivity (Newman et al., 2009). The heat Eq. (3) in a fuel pellet is discretized using the finite element method (FEM). To develop this approximation, the test space V is approximated by V^h using Lagrange finite elements such that $V^h\subset V$ and $V^h=\text{span}\{\phi_i\}_{i=1}^n$. The trial space hosting the macroscale solution is similarly approximated, where $v\in V^h$ is

$$v(\mathbf{x})=\sum_{j=1}^{n}v_j\phi_j(\mathbf{x}), \tag{5}$$

which allows the governing residual equations for heat conduction to be written in weak form as (Newman et al., 2009).

$$\mathbf{F}(T)=(k\nabla T^{k+1},\nabla\phi_i)-(Q,\phi_i)=\mathbf{0}. \tag{6}$$

BISON uses a preconditioned JFNK method (Knoll and Keyes, 2004) to solve (6). For more detail on the preconditioned JFNK algorithm, see Knoll et al. (2009).

3.2. Mesoscale model

As a simplified description of nuclear fuel, the radiation-induced microstructure evolution is represented by the phase field model developed by Rokkam et al. (2009). As such, the fuel is described as a generic, single component metal. Collision cascades from energized particles are assumed to only generate vacancies, neglecting other point defects. The microstructure evolves within a two-dimensional square domain with sides $l=1.28\,\mu$m defined by the radial and axial dimensions. The internal pellet temperature varies radially by approximately 200–250 K on the macroscale. Linearly scaling the macroscale temperature gradient to the mesoscale shows that the temperature will only vary by approximately 0.1 K across the mesoscale domain. Thus, this small mesoscale temperature gradient is neglected within the model.

In the model, vacancies are represented by a concentration field $c_v(\mathbf{r},t)$ and the void phase is defined by the continuous order parameter $0\le\eta(\mathbf{r},t)\le1$, where $\eta=0$ in the solid material and $\eta=1$ in a void. This phase field approach is based on defining a total free energy functional of the system such that two stable material phases are defined, the matrix phase ($\eta=0$ and $c_v=c_v^{\text{eq}}$) and the void phase ($\eta=1$ and $c_v=1$). The functional is then used to derive kinetic equations for c_v and η. The free energy of the non-uniform system is defined as

$$F(c_v,\eta)=N\int_V[h(\eta)G_v(c_v)+w(c_v,\eta)+\kappa_v(\nabla c_v)^2+\kappa_\eta(\nabla\eta)^2]dV, \tag{7}$$

where κ_v and κ_η are the gradient coefficients, N is the lattice site density of the material and $h(\eta)=(\eta-1)^2(\eta+1)^2$ is a shape function which varies continuously from 0 to 1. The interfacial energy contributions are defined by the two gradient terms. The free energy of the matrix phase G_v is derived in terms of the enthalpic and entropic contributions of the point defects as

$$G_v(c_v)=E_v^f c_v+k_bT[c_v\ln(c_v)+(1-c_v)\ln(1-c_v)] \tag{8}$$

with the vacancy formation energy E_v^f and Boltzmann constant k_b. The transition to the zero free energy in the void phase is defined by the Landau-type functional

$$w(c_v,\eta)=-A(c_v-c_v^{\text{eq}})^2\,\eta(\eta+1)(\eta-1)^2+B(c_v-1)^2\,\eta^2, \tag{9}$$

with coefficients A and B and the equilibrium vacancy concentration $c_v^{\text{eq}}\approx c_v^0\exp(-E_v^f/k_bT)$.

Following standard procedure in the phase field approach, the kinetic equations for the evolution of c_v and η are

$$\frac{\partial c_v}{\partial t}=\nabla\cdot M_v\nabla\frac{1}{N}\frac{\partial F(c_v,\eta)}{\partial c_v}+S_v(\mathbf{r},t), \tag{10}$$

$$\frac{\partial\eta}{\partial t}=-\frac{1}{N}L_v\frac{\partial F(c_v,\eta)}{\partial\eta}+S_v(\mathbf{r},t), \tag{11}$$

where $M_v=D_v/(k_bT)$ is the spatially independent vacancy mobility with the diffusivity $D_v=D_v^0\exp(E_v^m/k_bT)$ and L_v is the order

Table 1
Values for the mesoscale model parameters.

D_v^{0*}	3620.0	κ_v	0.5 eV/nm^2
c_v^0	1.0	κ_η	1.0 eV/nm^2
E_v^m	1.0 eV	P_{casc}	5.0×10^{-5}
E_v^f	1.0 eV	V_g^*	500.0
L_v	1.0	C_1	0.0375 mK/W
A	1.0 eV	C_2	2.165×10^{-4} m/W
B	1.0 eV	C_3	4.715×10^9 WK/m
dt^*	0.002	C_4	16,361 K
t^*_{max}	150.0		

parameter mobility. The stochastic driving force S_v represents the stochastic increase in the vacancy concentration due to irradiation. Its value is determined by P_{casc}, the probability of cascades occurring within a unit volume per time, and V_g, the maximum rate of increase in vacancy concentration during a time step, i.e.,

$$S_v(\mathbf{r}, t) = \begin{cases} 0 & \text{if } \eta > 0.8 \text{ or } R_1 > P_{\text{casc}} \\ R_2 V_g & \text{if } \eta \leq 0.8 \text{ or } R_1 \leq P_{\text{casc}} \end{cases}, \tag{12}$$

where R_1 and R_2 are random numbers generated uniformly between 0 and 1 at each time step and at each grid point. The condition that $\eta < 0.8$ for $S_v(\mathbf{r}, t) > 0$ ensures that cascades do not occur in the void phase. For more information about this model, see Rokkam et al. (2009).

For this work, (10) and (11) are uniformly discretized in space and solved using an explicit finite-difference approach with forward Euler time-stepping and periodic boundary conditions. The system is solved in reduced units (r.u.) of time,[2] such that the microstructure evolves for $t^*_{\text{max}} = 150.0$ r.u. with a time step $dt^* = 2 \times 10^{-3}$ r.u. Given a vacancy diffusivity for a specific material, the actual time is determined according to

$$t = \frac{t^*(10\,\text{nm})^2}{D_v}. \tag{13}$$

Table 1 summarizes the mesoscale model parameter values for the generic material used in this work. The values are such that the non-dimensionalized mobility $M_v^*(1100\,\text{K}) = 1.0$.

3.3. Multiscale coupling

The microstructure evolution predicted by the phase field model is temperature-dependent, due to the temperature dependence of the vacancy equilibrium concentration c_v^{eq}, the vacancy diffusivity D_v and the vacancy mobility M_v. Phase field simulations conducted with the conditions mentioned in the previous section, for identical time and radiation dose, show a significant increase in void fraction, or porosity, with increasing temperature above $T = 800$ K, as seen in Fig. 2. The porosity is higher at higher temperatures because the vacancy mobility is higher, thus accelerating the vacancy migration. Random scatter or roughness is also evident in the data, due to the random radiation source term S_v.

To calculate the effective thermal conductivity over an evolved microstructure, the spatially dependent mesoscale thermal conductivity $k'(\mathbf{r})$ must first be determined. To represent the thermal conductivity in the bulk of the model fuel, a temperature-dependent expression for the thermal conductivity in UO_2 (Lucuta et al., 1996) is used, i.e.,

$$k_{\text{bulk}} = \frac{1}{C_1 + C_2 T} + \frac{C_3}{T^2} \exp\left(-\frac{C_4}{T}\right), \tag{14}$$

where the parameter values are given in Table 1. Points at which the order parameter $\eta > 0.8$ are assumed to be in a void and the

[2] See Rokkam et al. (2009) for a detailed description of the non-dimensionalization of the phase field model.

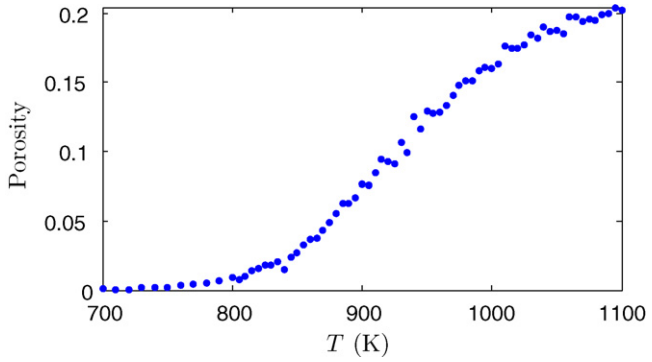

Fig. 2. The predicted void fraction, or porosity, in an irradiated material using the parameter values from Table 1 at various temperatures, but identical time and radiation dose. Note that each simulation is conducted using the same random seed in the pseudo-random number generation. The results show significant increase in the porosity with increasing temperature above $T = 800$ K.

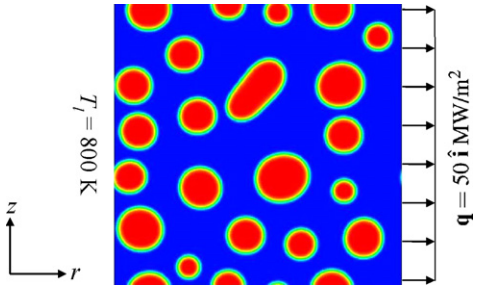

Fig. 3. A schematic of the method used to calculate the effective thermal conductivity k. k is determined by solving (16) with a constant temperature ($T_l = 800$ K) on the left boundary and a constant heat flux ($\mathbf{q} = 50\hat{\mathbf{i}}$ MW/m^2) applied to the right boundary.

void conductivity in this simple model is assumed to be that of He gas, $k_{\text{void}} = 0.152$ W/m K. Therefore, the mesoscale thermal conductivity is determined according to

$$k'(\mathbf{r}) = \begin{cases} k_{\text{bulk}} & \text{if } \eta \leq 0.8 \\ k_{\text{void}} & \text{if } \eta > 0.8 \end{cases}. \tag{15}$$

The effective thermal conductivity of the mesoscale microstructure after irradiation is determined with the technique employed by Millett et al. (2008). In this technique, the ability of the microstructure to conduct heat in the radial direction is measured with a virtual test procedure in which the left boundary is held at a constant temperature T_l and a test heat flux $\mathbf{q} = q_t\,\hat{\mathbf{i}}$ is applied over the right boundary as illustrated in Fig. 3. Periodic boundary conditions are applied over the top and bottom boundaries. The temperature field throughout the microstructure is determined by solving the steady-state heat conduction equation

$$\nabla \cdot (k'(\mathbf{r}) \nabla T) = 0 \tag{16}$$

using the same grid as that used for the phase field simulations. The effective conductivity is determined with the expression

$$k = -\frac{q_t}{\partial T / \partial x}, \tag{17}$$

where the derivative is approximated by

$$\frac{\partial T}{\partial x} \approx \frac{\bar{T}_r - T_l}{l} \tag{18}$$

with $\bar{T}_r$ the average temperature on the right boundary and l the side length. At the macroscale, (18) is exact since the mesoscale is

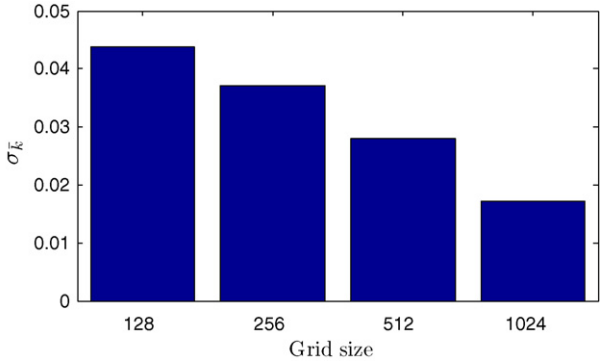

Fig. 4. Standard deviation of the random scatter in the thermal conductivity, $\sigma_{\bar{k}}$, determined by the mesoscale model for various grid sizes. The standard deviation decreases with increasing grid size.

measure zero, i.e.,

$$\frac{\partial T}{\partial x} = \lim_{l \to 0} \frac{\bar{T}_r - T_l}{l}. \tag{19}$$

In this work, the values $T_l = 800\,\mathrm{K}$ and $q_t = 50\,\mathrm{MW/m^2}$ are used, however these values are arbitrary and have no effect on the value of the calculated thermal conductivity.

The random radiation term S_v from (10) introduces random noise into the mesoscale calculation, as seen in the calculated porosity (see Fig. 2). To investigate to what extent increasing the domain size reduces the magnitude of the roughness in the calculated thermal conductivity, the value of k is computed with the mesoscale model over a narrow band of temperatures ($999.9 \leq T \leq 1000.1$) using differing spatial domain sizes ranging from 128×128 to 1024×1024, keeping the distance between grid points constant. The roughness in the mesoscale-calculated value of k is quantified by calculating its standard deviation.

Fig. 4 shows that the standard deviation decreases with increasing grid size, such that there exists a domain size where the randomness will no longer impact the convergence rate of the multiscale solution. However, given the computational cost of increasing the domain size, this is not a viable means of eliminating the random noise in the effective thermal conductivity.

As discussed in Section 2, the values of the effective material parameters are dynamically fitted with a polynomial to eliminate this random noise. The curve-fit is improved at each nonlinear iteration, as more values are calculated by the mesoscale model. In this simulation, the effective thermal conductivity at each temperature are fitted with a fourth-order polynomial. Fig. 5 demonstrates the progress of the curve-fit during the nonlinear iteration.

3.4. Numerical performance

To investigate the performance of the multiscale model, two simulations are conducted, one to evaluate the nonlinear convergence and the other the parallel scalability of the approach. The mesoscale calculations employ the parameters from Table 1 to predict the void formation in the 2-D square of material discretized with a 128×128 finite-difference grid.

The first simulation considers the pellet with a constant temperature $T_C = 810\,\mathrm{K}$ on the outer circumference and a uniform applied heat source $Q = 200\,\mathrm{MW/m^3}$. The pellet is discretized with 720 elements and the temperature distribution throughout the pellet is calculated using the multiscale model. Fig. 6 shows the strong nonlinear convergence obtained by the proposed multiscale JFNK approach on this representative problem.

To evaluate the parallel scalability of the basic scale-bridging methodology suggested here, the pellet is maintained at a constant

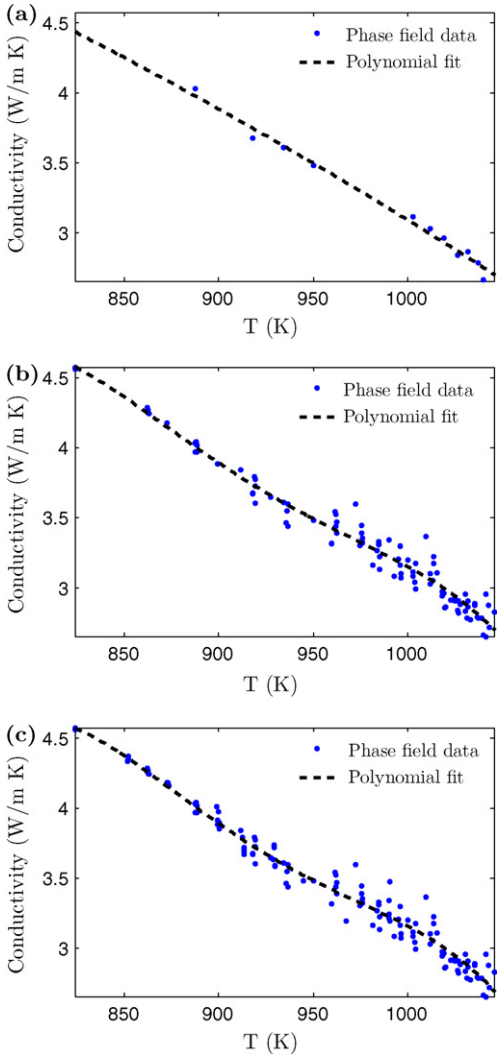

Fig. 5. The progress of the dynamic curve-fit of the thermal conductivity calculated by the mesoscale model during the JFNK solution, where (a) is the fit after the first nonlinear iteration, (b) is the fit after the third iteration, and (c) is the fit after the fifth iteration. Note that each successive curve-fit considers all values of k calculated during previous time steps.

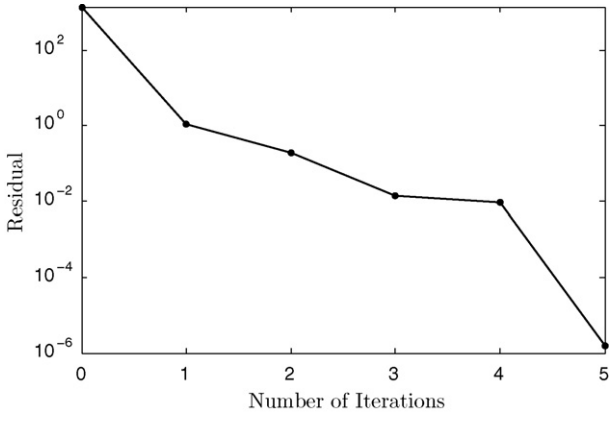

Fig. 6. Plot of the nonlinear residual vs. number of Newton iterations during the multiscale simulation. The model exhibits good nonlinear convergence.

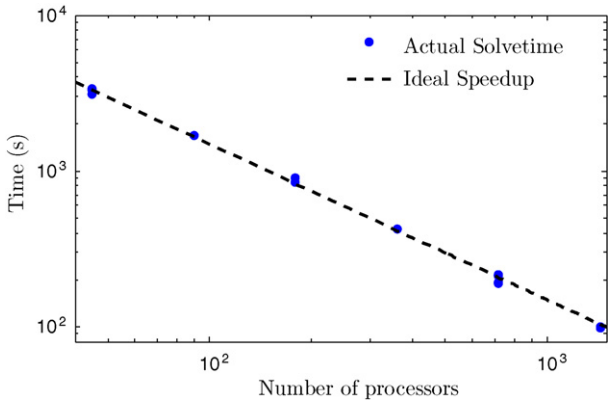

Fig. 7. The parallel scalability of the multiscale calculation. The problem size is kept constant as the number of processors is increased. The multiscale model exhibits near ideal scalability.

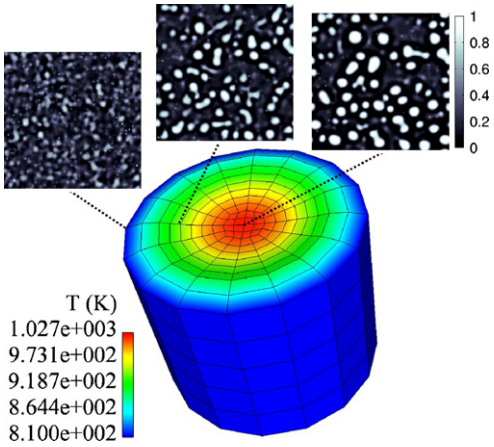

Fig. 8. Computed fuel pellet temperature profile, where color corresponds to temperature. Snapshots above the pellet show vacancy concentration in the microstructure computed by the mesoscale model at the indicated radial positions.

temperature $T = 810$ K. For this simulation, the pellet is discretized with 5760 elements and the mesoscale model is evaluated once per integration point, as only one iteration is required. The "strong" parallel scalability is investigated, i.e., the problem size is unchanged while it is solved using an increasing number of processors ranging from 3 to 1440. The method exhibits near ideal scalability, as shown in Fig. 7. This result is not surprising, as each mesoscale calculation is independent from the others, and run concurrently within each JFNK function evaluation.

3.5. Results

In the previous section, the multiscale model was shown to have good nonlinear convergence and excellent parallel scalability. In this section, the physical behavior predicted by the mesoscale model is investigated. The fuel pellet simulation used to investigate the nonlinear convergence is repeated here, i.e., the temperature profile is determined in a fuel pellet of height $h = 6.75$ mm and diameter $d = 8.26$ mm with a constant temperature $T_C = 810$ K on the outer circumference and a uniform applied heat source $Q = 200\,\mathrm{MW/m^3}$. The pellet is discretized with 720 elements and the mesoscale model is solved in the manner detailed in the previous section.

Fig. 8 shows both the temperature profile within the fuel pellet and plots of the mesoscale vacancy concentration at three radial positions within the pellet. From these results, it is evident that

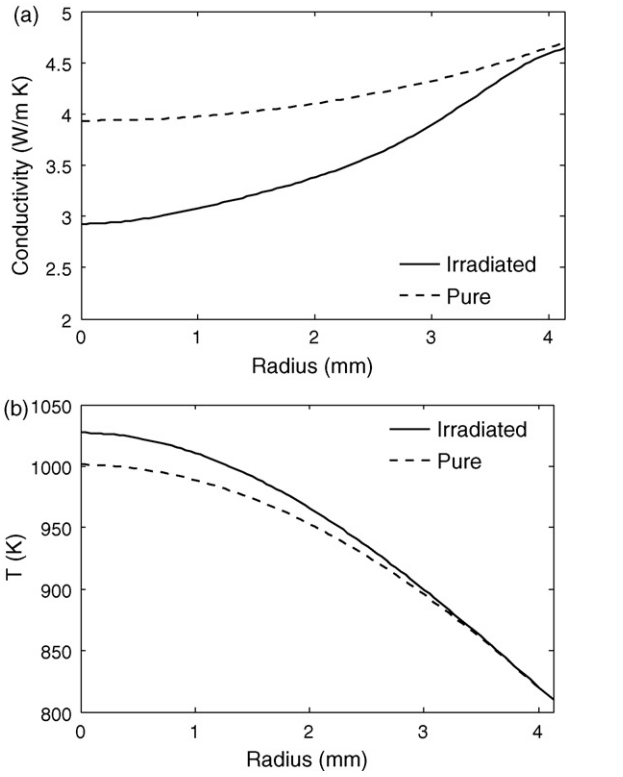

Fig. 9. Comparison between (a) the thermal conductivity and (b) the temperature profile at various radii in an irradiated fuel pellet and in a pure pellet. Values are measured at a height $z = 3.825$ mm from the base of the pellet.

the void formation has a strong radial dependence; at the pellet center, many large voids surrounded by vacancy-depleted zones have formed; at mid-radius, a larger number of small voids have formed; on the outer circumference, only a few small voids are present (see Sens (1972) for experimental observations showing similar behavior). Thus, the multiscale model explicitly determines the microstructure throughout the fuel pellet.

The radial variation in void formation results in radial variation in thermal conductivity. The effect of void formation on thermal conductivity and the pellet temperature is demonstrated by comparing the results to an unirradiated pellet in which the thermal conductivity is determined with (14). The values of the thermal conductivity and the temperature at various radii for the irradiated and the pure, unirradiated pellets are shown in Fig. 9(a) and (b), respectively.

Due to large voids in the center of the irradiated pellet, the thermal conductivity is significantly lower than that in the pure pellet. On the cooler outer edge, where only a few small voids have formed, the thermal conductivity is only slightly lower than that in the pure pellet. The low internal thermal conductivity reduces the transfer of heat to the pellet surface, and therefore the center temperature is 27 K hotter in the irradiated pellet than in the pure pellet. While quite simple due to the elementary models employed at both scales, these results reflect general behavior observed in fission reactors.

Due to the simple nature of this initial multiscale model, the mesoscale model can be decoupled from the macroscale and used to precalculate the relationship between thermal conductivity and temperature in the irradiated material, providing curve-fits similar to Fig. 5. These fits, in equation form, can then be independently used in the macroscale calculation. However, in a more complex transient problem where the mesoscale model is history dependent and influenced by several variables such as temperature, neutron flux, and density, precalculating the thermal conductivity would be

difficult due to the dimension of the state space that must be sampled. In such a case, or when details on the microstructure evolution are required, a coupled approach is necessary. The fully coupled multiscale model presented in this work is general and fully consistent; it can be used for simple problems, as demonstrated here, and also for complex, transient problems.

4. Conclusion

This work presents a methodology for coupling an FE fuel performance code to a mesoscale irradiated microstructure model to capture the effect of radiation-induced microstructure evolution on reactor performance. The FE model represents the fuel pellet, while the mesoscale model evolves the microstructure at each integration point and calculates effective material parameters. The multiscale nonlinear system is solved via a JFNK algorithm, where the mesoscale state is self-consistently coupled to the global solution by being evaluated within the function evaluation. To mitigate the effect of random noise in the calculated effective material properties on convergence rate, a dynamic curve-fitting approach fits a surface to the calculated values that gradually improves in accuracy until the solution converges. The curve-fit also serves to significantly reduce the total number of mesoscale calculations by adaptively focusing new calculations where data is needed, thereby making the multiscale solution more economical.

The multiscale approach is demonstrated on a simple model of a reactor fuel pellet. INL's BISON fuel performance code calculates the steady-state temperature profile in a fuel pellet. The effective thermal conductivity due to radiation is calculated with a simple phase field model of irradiated microstructures (Rokkam et al., 2009). The proposed multiscale approach demonstrates good nonlinear convergence and parallel scalability on a multiprocessor simulation of the simplified fuel pellet. Radial dependence of void formation on mesoscale temperature results in a lower thermal conductivity in the center of the pellet than in a similar, unirradiated pellet, and therefore a higher internal temperature. While an engineering-scale calculation could capture the effect of irradiation on thermal conductivity using an empirical fit of experimental data, only a multiscale approach, as presented here, can demonstrate the microstructure-based cause of this effect. Having demonstrated the viability of this fully coupled approach on a simplified fuel pellet model, more accurate pellet representations are being developed. The macroscale problem will include more accurate boundary conditions, transient heat conduction and fuel/cladding interactions. In addition, a more detailed mesoscale model will describe a specific model fuel material, such as UO_2. This includes the consideration of self-interstitials as well as vacancies, composition changes, fission gas and fission product migration, polycrystalline materials, electrostatics and the effect of stress and temperature gradients. The model fuel material will provide a specific time scale, as shown in (13), which can be compared to experimental results. Also, other material parameters, including density and elastic constants, will be passed between the macro- and mesoscales.

Acknowledgments

The authors wish to thank Anter El-Azab and Srujan Rokkam of Florida State University for useful discussions regarding the scale-bridging and phase field model. This work was supported by the US DOE, Office of Nuclear Energy Advanced Fuel Cycle Initiative under contract no. DEAC07-05ID14517 (INL/JOU-09-16784).

References

Allison, C.M., Berna, G.A., Chambers, R., Coryell, E.W., Davis, K.L., Hagrman, D.L., Hagrman, D.T., Hampton, N.L., Hohorst, J.K., Mason, R.E., McComas, M.L., McNeil, K.A., Miller, R.L., Olsen, C.S., Reymann, G.A., Siefken, L.J., 1993. SCDAP/RELAP5/MOD3.1 code manual, volume IV: MATPRO—a library of materials properties for light-water-reactor accident analysis. Tech. rep., NUREG/CR-6150, EGG-2720.

Beaudoin, A.J., Mathur, K.K., Dawson, P.R., Johnson, G.C., 1993. Three-dimensional deformation process simulation with explicit use of polycrystal plasticity models. Int. J. Plasticity 9 (7), 833–860.

Bochev, P., Christon, M., Collis, S., Lehoucq, R., Shadid, J., Slepoy, A., Wagner, G., June 2004. A mathematical framework for multiscale science and engineering: the variational multiscale method and interscale transfer operators. Tech. Re SAND2004–2871, Sandia National Laboratories.

Gaston, D., Newman, C., Hansen, G., Lebrun-Grandié, D., 2009. MOOSE: a parallel computational framework for coupled systems of nonlinear equations. Nucl. Eng. Des. 239, 1768–1778.

Habraken, A.M., Duchene, L., 2004. Anisotropic elasto-plastic finite element analysis using a stress–strain interpolation method based on a polycrystalline model. Int. J. Plasticity 20, 1525–1560.

Knoll, D., Park, R., Smith, K., 2009. Application of the Jacobian-free Newton-Krylov method in computational reactor physics. In: American Nuclear Society 2009 International Conference on Advances in Mathematics, May 3–7 Computational Methods, and Reactor Physics, Saratoga Springs, NY.

Knoll, D.A., Keyes, D.E., 2004. Jacobian-free Newton-Krylov methods: a survey of approaches and applications. J. Comput. Phys. 193 (2), 357–397.

Lucuta, P.G., Matzke, H.J., Hastings, I.J., 1996. A pragmatic approach to modelling thermal conductivity of irradiated UO_2 fuel: review and recommendations. J. Nucl. Mater. 232, 166–180.

Michopoulos, J., Farhat, C., Fish, J., 2005. Modeling and simulation of multiphysics systems. J. Comput. Inf. Sci. Eng. 5 (3), 198.

Millett, P.C., Wolf, D., Desai, T.D., Rokkam, S., El-Azab, A., 2008. Phase-field simulation of thermal conductivity in porous polycrystalline microstructres. J. Appl. Phys. 104, 033512.

Newman, C., Hansen, G., Gaston, D., 2009. Three dimensional coupled simulation of thermomechanics, heat, and oxygen diffusion in UO_2 nuclear fuel rods. J. Nucl. Mater. 392, 6–15.

Oh, J., Koo, Y., Lee, B., 2009. Simulation of high burnup structure in UO_2 using Potts model. Nucl. Eng. Technol. 41 (8), 1109–1114.

Olander, D.R., 1976. Fundamental Aspects of Nuclear Reactor Fuel Elements. Technical Information Center, Energy Research and Development Administration.

Rokkam, S.K., El-Azab, A., Millett, P.C., Wolf, D., 2009. Phase field modeling of void nucleation and growth in irradiated metals. Model. Simul. Mater. Sci. Eng. 17, 064002.

Ropp, D.L., Shadid, J.N., 2005. Stability of operator splitting methods for systems with indefinite operators: Reaction-diffusion systems. J. Comput. Phys. 203 (2), 449–466.

Ropp, D.L., Shadid, J.N., Ober, C.C., 2004. Studies of the accuracy of time integration methods for reaction-diffusion equations. J. Comput. Phys. 194 (2), 544–574.

Sens, P., 1972. The kinetics of pore movement in uo2 fuel rods. Journal of Nuclear Materials 43 (3), 293–307.

Tikare, V., Holm, E., 1998. Simulation of grain growth and pore migration in a thermal gradient. J. Am. Ceram. Soc. 81 (3), 480–484.

Yu, Q., Fish, J., 2002. Multiscale asymptotic homogenization for multiphysics problems with multiple spatial and temporal scales: a coupled thermo-viscoelastic example problem. Int. J. Solids Struct. 39, 6429–6452.